Preprint
UCRL-JC-139120

The Completeness Criterion in Atomic Modeling

D. Liedahl

This article was submitted to *Atomic Data Needs for X-Ray Astronomy: Proceedings, Greenbelt, MD, December 16-19, 1999*

April 3, 2000

U.S. Department of Energy

Lawrence
Livermore
National
Laboratory

This work was performed under the auspices of the United States Department of Energy by the University of California, Lawrence Livermore National Laboratory under contract No. W-7405-Eng-48.

The Completeness Criterion in Atomic Modeling

Duane A. Liedahl

Physics Department, Lawrence Livermore National Laboratory
P.O. Box 808, Livermore, CA 94550, duane@virgo.llnl.gov

Abstract. I discuss two variations on the completeness theme in atomic modeling; missing lines as they affect the performance of spectral synthesis codes, and missing configurations as they affect the theoretical emissivities of bright lines, with emphasis on the latter. It is shown that the detrimental effects of working with incomplete atomic models can overshadow those brought about by working with less-than-perfect atomic rates. Atomic models can be brought up to an acceptable level of completeness in a fairly straightforward manner, and on a reasonably short timescale, whereas the long-term goal of comprehensive accuracy is unlikely to be reached on the timescale of the current generation of X-ray observatories. A near-term, albeit imperfect, solution is to hybridize atomic models used to synthesize spectra. A hybrid atomic model is one for which a large-scale atomic model, in which completeness is achieved at the expense of accuracy, is augmented with more accurate atomic quantities as they become available.

1. MISSING LINES AND SPECTRAL SYNTHESIS CODES

Atomic and spectral databases have a variety of practical uses in X-ray astronomy. For example, since identifying bright lines and evaluating any potential problems associated with line blending are often the first steps in analyzing high-resolution spectra, access to a wavelength-ordered compilation of spectral lines greatly facilitates any first-pass interpretation. But even the nominally simple task of line identification cannot be wholly decoupled from assessments of relative line intensities. Moreover, the goals of X-ray spectroscopists are, fortunately, more ambitious than simple line labeling. In collisionally-ionized plasmas, to which this article is restricted, we are thus brought up against the complexities of calculating collision strengths. In most X-ray spectra, there will be only a handful (say, a few tens or less) of bright lines. Since bright lines are less affected by background contamination and counting statistics than faint lines, they will usually be chosen over faint lines to aid in deriving physical constraints. Therefore, it is only natural that we should first devote our limited resources to improving the subset of the atomic collision database relevant to those bright lines.

The luxury of ignoring the hundreds (if not thousands) of weak lines that accompany the bright lines is one afforded us by the advent of high resolution X-ray spectroscopy. By contrast, with low-to-moderate spectral resolution, such as that available with CCDs, we need the capability to reproduce the entirety of an X-ray spectrum. While it is true that the ensemble of bright lines carries most of the line power in the X-ray band, it is *not* true on a bin-by-bin basis. If weak lines are ignored or otherwise improperly taken into account, *data* $-$ *model* residuals can frustrate attempts at χ^2 fitting. There is no choice but to treat weak lines. This presents a formidable challenge, entailing the generation and management of a vast quantity of atomic data.

Spectral synthesis codes (SSCs) provide a convenient way to access and process atomic databases. In particular, SSCs allow the efficient generation of theoretical spectra. Various pieces of evidence obtained over the last few years, however, indicate that X-ray SSC databases are, in a practical sense, incomplete, a lesson brought to us by *ASCA* [4] and *EUVE* [18]. Note that while the *ASCA* era may be drawing to a close, we will not be leaving the CCD era behind, given the prominent role that the *Chandra* ACIS and *XMM* EPIC instruments are sure to play in X-ray astronomy over the next decade. Thus it remains imperative that the deficiencies identified from earlier studies be fully redressed. It may seem ironic that spectral data in which much of the detail is obscured forces spectral modelers into the most detailed considerations of spectral formation.

The SSC incompleteness problems that have been identified involve the absence of emission lines $-$ the "missing line" problem [3] [15]. In terms of atomic modeling, the missing line problem is equivalent to missing energy levels. Radiative transitions from those levels, were they included, would add a substantial contribution

to the total radiative power currently represented in plasma codes. The spectral distribution of the missing flux is non-trivial. In the case of Fe L-shell line emission, it has been found that $n \rightarrow 2$ ($n \geq 6$) emission resolves earlier problems in fitting plasma models to *ASCA* data in the 1.0–1.5 keV range (Liedahl & Brickhouse, in prep; [4]). For the remainder of this article, I want to take the missing line problem as a "given," and then focus on another (related) problem.

2. MISSING ENERGY LEVELS AND LEVEL POPULATION KINETICS

The missing lines are, individually, more or less unobservable; it is only their aggregate effect that becomes a concern. Of course, were they individually observable they would not have qualified as "missing" for so long. In this section it is shown that even bright-line emissivities can be substantially affected by configurations that are typically left out of calculations. It is often the case that atomic models constructed for the purpose of calculating $n \rightarrow n'$ spectra ignore configurations with electrons in $n+1, n+2$, etc. For the purposes of this discussion, I will refer to such a model as a *minimal model*. A trivial example of a minimal model would be the 4-level H-like ion, consisting of $1\ ^2S_{1/2}$, $2\ ^2S_{1/2}$, and $2\ ^2P_{1/2,3/2}$, which would allow a simplified calculation of $n = 2 \rightarrow n = 1$ spectra. For some bright lines (say, $u \rightarrow \ell$, with the energy of the upper level u denoted by $E(u)$, etc.), the neglect of higher energy levels causes no problem, if u is populated almost exclusively by electron impact excitation from ground ($ground \rightarrow u \rightarrow \ell$). For others, however, which may depend largely upon indirect population flux paths [$ground \rightarrow k \rightarrow u \rightarrow \ell$, where $E(k) > E(u)$], the calculated line emissivities will vary according to the completeness of the atomic model, and will simply be wrong when using the minimal model. The essential point is, therefore, that

model size alone has a bearing on the outcome of spectral simulations.

Two examples are presented below, Ne-like Fe XVII and Ar-like Fe IX. Admittedly, many of the collisional rate coefficients will not be highly accurate (approximately 2,000,000 electron impact cross-sections were calculated for Fe IX), since no attempt was made to include resonances in the cross-sections. The intention is to compare calculations made with the same set of atomic codes, so as to isolate model size as the only variable. All calculations were performed with the HULLAC (Hebrew University/Lawrence Livermore Atomic Code) atomic physics package [2] [14]. Atomic structure is calculated using a relativistic parametric potential in intermediate coupling. Radiative rates include the multipoles E1, E2, M1, and M2. Collisional rate coefficients are obtained by integrating quasi-relativistic distorted wave cross-sections over a Maxwellian electron distribution. Steady-state level populations relative to ground are determined through inversion of the rate matrix, assuming no coupling to adjacent charge states. Line powers then follow from the level populations and radiative rates.

2.1 Ne-like Fe XVII

With its closed shell ground configuration, Ne-like Fe XVII exists across a broad temperature range, and attains a high ionic fraction near its temperature of peak abundance [1]. Its $n = 3 \rightarrow n = 2$ lines fall into the 15–17 Å band, and are often among the brightest seen in solar [16] [17] and stellar [6] [7] X-ray spectra. Models for this ion suffer from a number of problems — lack of resonances in the collisional excitation cross-sections, neglect of dielectronic recombination on level populations, and neglect of inner-shell ionization of Na-like iron in creating Ne-like $2p^5 3s$, to name a few. In studying the $n = 3 \rightarrow n = 2$ emission spectrum, the minimal model is sometimes still employed. Here I will address only the effects on Fe XVII modeling of using the minimal model.

Three of the bright Fe XVII lines originate in the lowest excited configuration $2s^2 2p^5 3s$. The four levels inside this configuration have total angular momenta $J = 2, 1, 0, 1$, in ascending energy order. The electric dipole transitions of the two $J = 1$ levels to the $2s^2 2p^6$ ($J = 0$) ground level are responsible for bright lines at 16.77 Å and 17.05 Å. The $J = 2$ level, being the first excited level, has nowhere to go but to ground, and so decays by a slow M2 transition, producing the bright 17.10 Å line. For convenience, these lines are sometimes designated 3F (16.77 Å), 3G (17.05 Å), and M2 (17.10 Å).

The minimal Ne-like iron model consists of 37 levels distributed among the configurations $2s^2 2p^6$ and $(2s2p)^7\ 3l$. To illustrate the effect on predicted line powers of varying the model size, four additional HULLAC models were assembled by successively adding shells to the minimal model, up to and including $n = 7$. For each model the temperature is set to $kT = 500$ eV. The results for the line powers of 3F, 3G, and M2 are

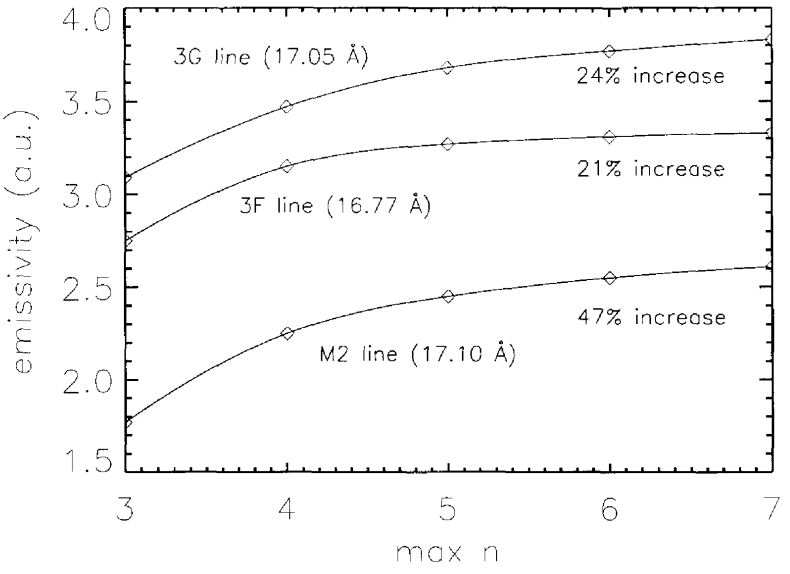

FIGURE 1. Predicted relative emissivities of three bright Fe XVII (Ne-like) lines for five different models, plotted as continuous curves for clarity. The low-density limit and an electron temperature $kT = 500$ eV are assumed. All three lines (wavelengths and common designations shown) arise from transitions of the type $2s^2 2p^6 - 2s^2 2p^5 3s$. The models are characterized by the value of the highest included shell (x-axis). The percent increases in line power, comparing the $n = 7$ to the $n = 3$ models, are indicated.

plotted against the highest included principal quantum number in Figure 1. First, note that the line powers increase most rapidly with model size in going from $n_{\max} = 3$ to $n_{\max} = 4$; addition of "nearby" levels has a more pronounced effect than adding "distant" levels. Second, the curves show signs of converging; adding shells beyond $n = 7$ will have a small effect. In fact, reasonable convergence is obtained for $n_{\max} = 5$. Finally, note that the line powers increase by differing amounts. While the 3F/3G ratio is roughly constant with $n_{\max}$, the M2/3G (M2/3F) ratio changes from 0.56 (0.64) to 0.68 (0.79) in going from $n_{\max} = 3$ to $n_{\max} = 7$. We remind the reader that the values of these ratios should not be taken too seriously, since, as mentioned earlier, the presence of adjacent charge states has not been taken into account. In other words, the ratios are not strictly independent of temperature. Since Fe XVII is a dominant ion in X-ray spectra, used for determining temperatures, iron abundance, and, in solar coronal studies, the effects of resonant scattering, the errors inherent in the use of the minimal model cannot be dismissed.

2.2 Ar-like Fe IX

Similar to Ne-like iron, Ar-like Fe is the dominant iron ion near its temperature of peak abundance, owing to its closed $3p$ subshell. In the EUV range the brightest Fe IX lines have upper levels distributed among the twelve excited levels in the first excited configuration $3s^2 3p^5 3d$. Only the three $J = 1$ levels in $3s^2 3p^5 3d$ are connected to the $J = 0$ ground via dipole-allowed transitions — $\lambda\lambda$ 171.1 (from level 13), 217.1 (level 10), and 244.9 (level 3), respectively. By far, the most readily observable Fe IX line is $3p^6\ ^1S_0 - 3p^5 3d\ ^1P_1$ λ171.1. Since it is bright, it is the most important proxy for Fe^{8+}, and is used to constrain the emission measure distribution near 10^6 K. Next in importance are the pair of lines just longward of 240 Å; the M2 line from level 4, $3p^6\ ^1S_0 - 3p^5 3d\ ^3P_2$ λ241.7; and $3p^6\ ^1S_0 - 3p^5 3d\ ^3P_1$ λ244.9. The ratio of these two lines (denoted by 241.7/244.9)

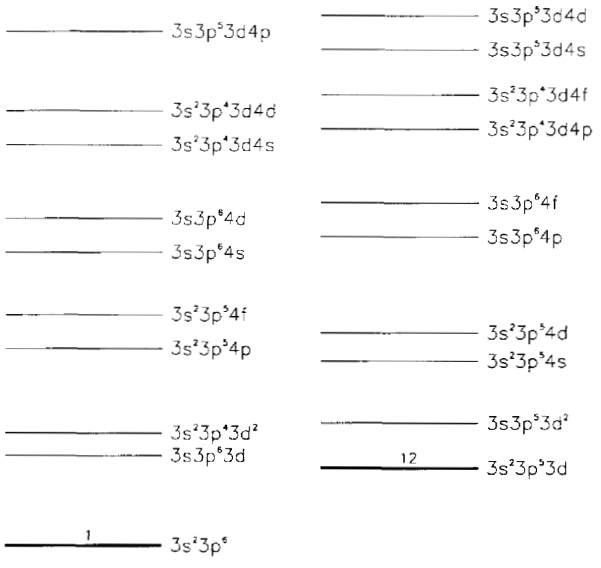

FIGURE 2. Schematic of 1067-level HULLAC model of Ar-like Fe IX. Even parity configurations are on the left, those of odd parity are on the right. The vertical positioning represents the relative positions (not to scale) of configuration-averaged energies. The '1' and '12' signify the number of fine-structure energy levels corresponding to the $3s^2 3p^6$ and $3s^2 3p^5 3d$ configurations, respectively. Current spectral code predictions are based either upon a 13-level Fe IX model consisting of these two configurations alone (*darkened lines*), or a 17-level model that includes the four levels inside $3s^2 3p^5 4s$.

serves as a density diagnostic for densities characteristic of stellar coronae [12]. In this section, I will emphasize the line powers of these two lines compared to each other and compared to λ171.1.

Apparent inconsistencies between theoretical predictions and observed Fe IX spectra have been noted in the literature. The ratios 241.7/171.1 and 244.9/171.1 have been reported as being much larger than emission code predictions [5] [9]. Also, the ratio 241.7/244.9 appears to imply higher densities than inferred from neighboring ions [8] [11] (cf., [13]). While these two discrepancies are related, and the results shown below are relevant to both problems, only the latter issue will be addressed in detail here. Not surprisingly, in modeling these three lines, the minimal Fe IX model [10] is the one most commonly used (e.g., [5]). It consists of the thirteen levels belonging to the ground and first excited configurations.

To determine whether or not the theoretical line powers of the three Fe IX lines mentioned above also depend on model size, we perform an "experiment" similar to that described in the previous section. Using HULLAC, a minimal 13-level model and a larger model (1067 levels) were constructed. The set of configurations included are displayed in Figure 2. The 13-level ion results from stripping the larger model of all energy levels not belonging to $3s^2 3p^6$ or $3s^2 3p^5 3d$. This procedure, as opposed to simply constructing a 13-level model from scratch, removes any differences in calculated rates that might arise from the effects of configuration interaction. Any disagreements in predicted line emissivities between the two models thus reflect differences in the level population kinetics. In terms of accuracy, rate by rate, the distorted wave calculations will not be highly reliable, as they do not treat resonances in the cross-sections, which are important for this ion (P. Storey, priv. comm.). Therefore, to make the experiment meaningful, HULLAC models are compared only to other HULLAC models. This eliminates any ambiguity that might arise from using different atomic datasets. Therefore, the results presented here should be *qualitatively* robust against changes in the set of rate coefficients.

Probably the most essential improvement in the 1067-level model compared to the 13-level model is the inclusion of the 111 levels inside of the $3s^2 3p^1 3d^2$ configuration, which provide important sinks for $3s^2 3p^5 3d$ levels. Note, however, that the model is still far from complete, as it lacks configurations with principal quantum numbers greater than 4, and does not account for interactions with adjacent charge states. If our intuition derived from studying Fe XVII can be trusted, adding a fifth shell, sixth shell, and so on will become less and

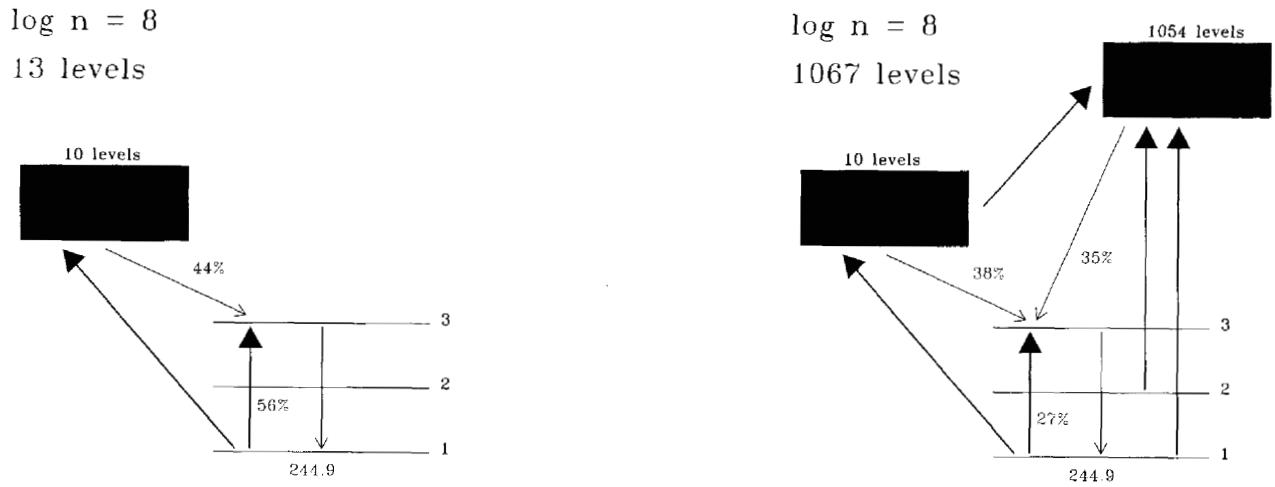

FIGURE 3. Schematic of level population kinetics leading to emission of λ244.9 in Ar-like Fe IX, illustrating the dependence on model size (*left panel*: 13 levels; *right panel*: 1067 levels) of the relative weightings of various population flux paths. An electron density of 10^8 cm^{-3} is assumed (cf., Fig. 4). Levels 1, 2, and 3 are $3s^2 3p^6\ ^1S_0$ (ground), $3s^2 3p^5 3d\ ^3P_0$, and $3s^2 3p^5 3d\ ^3P_1$, respectively. The remaining 10 levels of $3s^2 3p^5 3d$ are grouped and symbolized as the box on the left of each diagram. The remaining 1054 levels, spread among the remaining configurations shown in Fig. 2, are grouped and represented by the box on the right side of the right panel. Heavy arrows represent collisional transitions, while the lighter arrows represent radiative transitions. Percent values show relative contributions to population influx to level 3 along various pathways.

less important, and adding the fourth shell, as we have done here, should go a long way toward accounting for the population kinetics responsible for production of the three lines under consideration.

Tracing population flux paths in Fe IX, even for the 13-level ion, is quite involved. To simplify the description,

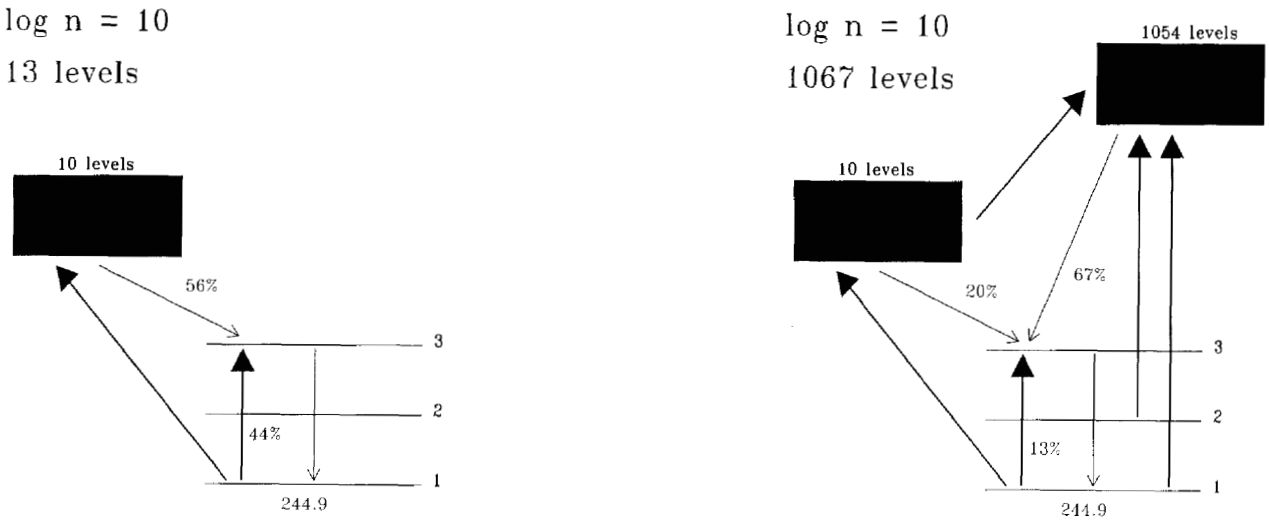

FIGURE 4. Schematic of level population kinetics in Ar-like Fe IX assuming an electron density of 10^{10} cm^{-3}. See the figure caption to Fig. 3 for additional explanation.

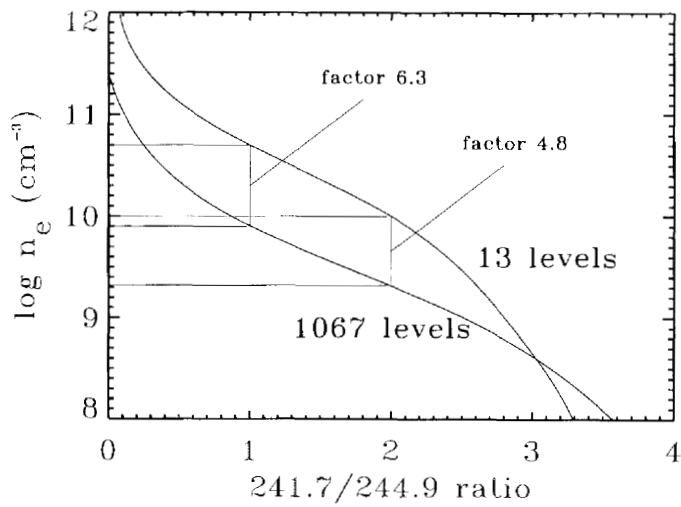

FIGURE 5. Behavior of the Fe IX 241.7/244.9 emissivity ratios vs. electron density, as determined from two models of the ion which differ in the number of levels included in the rate equations. Coordinate axes are reversed so that, from a hypothetical observed value of the ratio, one reads off the density from the y-axis. Note that use of the smaller model leads to an overestimate of the density for ratios less than 3.0. Two examples are shown: a ratio of 1.0 would imply densities varying by a factor of 6.3, depending on which model is used; a ratio of 2.0 implies densities that vary by a factor of 4.8.

highly schematized diagrams (Figures 3 and 4) are used. Focusing on $^3P_1$ (level 3), Figure 3 shows the percent contributions to the population influx at a density of 10^8 cm^{-3} for the two models. Even at this relatively low density, near the lower end of solar coronal densities, the additional configurations can be seen to play an essential role in determining the level 3 population. For example, in the 13-level model, 56% of the influx is attributed to collisional transitions from ground, while in the 1067-level model, this percentage is only 27%. Also note that $^3P_0$ (level 2), whose radiative decay to ground is strictly forbidden, finds important depopulation channels among $3s^2 3p^1 3d^2$. Some of this population flux ends up in level 3, illustrative of the "recirculation" of population that the new configurations allow. Increasing the density to 10^{10} cm^{-3} (see Figure 4) increases the fraction of population influx that that is channeled through the new set of configurations. The contrast of the relative importance of direct excitation from ground is larger than in the lower-density case.

In terms of the brightness of λ244.9 relative to λ171.1, the net result of adding the new set of configurations is that the ratio 244.9/171.1 is a factor of 2–3 times higher than predicted using the 13-level model. A similar result is found for λ241.7, although its behavior is more complex. In Figure 5, the 241.7/244.9 ratio is plotted against density for the two models. Over the range of density for which this ratio is especially useful, i.e., where both lines are observable and sensitive to density variations, the two models provide substantially discrepant results. For a given observed line ratio the 13-level model leads to an overestimation of the density by factors of a few (see Figure 5). Therefore, use of the larger model partially (if not entirely) alleviates the observed inconsistencies.

A more complete treatment of Fe IX level population kinetics will appear in a future paper (Liedahl, Mewe, & Kaastra, in preparation). Detailed calculations using the R-matrix technique have shown that qualitatively similar corrections to the theoretical line ratios result from the use of more accurate cross-sections (P. Storey, priv. comm.). Studies of the combined effects of better cross-sections and a better treatment of the level population kinetics should prove interesting.

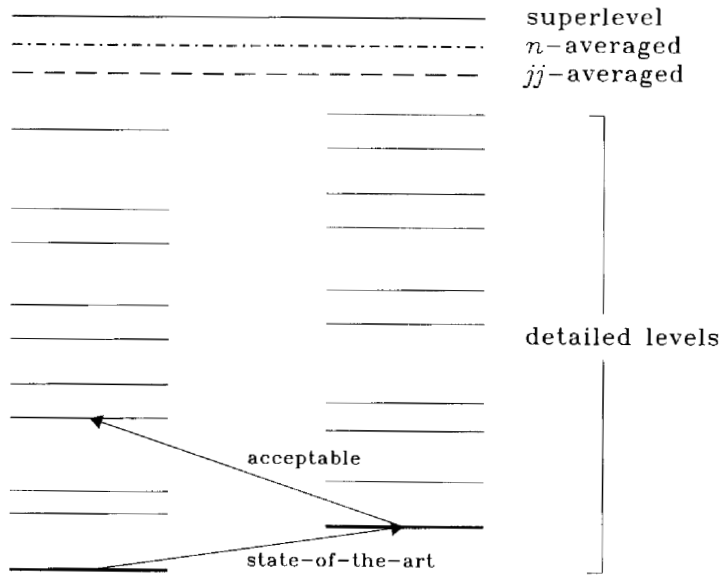

FIGURE 6. Schematic diagram of a hybrid atomic model, built around the detailed Ar-like Fe IX level structure, represented in Fig. 2. Detailed levels are coupled to all other accessible detailed levels by collisional and radiative transitions. A set of jj-averaged 'levels' (*dashed line*) consist of artificial levels that lump together detailed levels sharing a relativistic configuration. A set of n-averaged 'levels' (*dash-dotted line*) result from lumping levels that share a common set of principal quantum numbers. A 'superlevel' represents the remainder of the atomic structure, and is usually included to account for levels characterized by very high principal quantum numbers and their interactions with lower levels, as well as with adjacent charge states. The arrows represent collisional excitation rate coefficients. The enormous number of cross-sections required for a model of this size means that only a subset of the rates can be of 'state-of-the-art' quality. For the rest, we can settle for 'acceptable' rates, but should not settle for the absence of rates.

3. SUMMARY OF PROBLEMS AND A PROPOSED FIX

Moderate resolution — weak lines. Experiences with *ASCA* spectra have shown that the absence of weak lines, even though they may be individually unimportant, compromises our ability to obtain broadband fits to spectroscopic data of low-to-moderate resolution. The spectral distribution of missing lines is poorly known, and has been investigated quantitatively only for a few iron L-shell ions. Broadband fitting places high demands on plasma emission codes, requiring completeness down to the level of statistical or instrumental uncertainties. This problem will resurface in force in the near future, when data from the *Chandra* ACIS and *XMM* EPIC instruments become widely available.

High resolution — strong lines. It might seem that, in dealing with high-resolution data, completeness takes a back seat to accuracy, since we can dispense with broadband fits, and concentrate on our favorite handful of lines. There is a different kind of completeness, however, discussed in §2 — the completeness of atomic models. For at least for two important cases, I have shown that the use of incomplete models will lead to significant errors, regardless of the degree of accuracy of the rates contained therein.

To begin to remedy these problems, first, it should be recognized that the benefits of replacing moderate-quality atomic data with high-quality data can be overshadowed by effects arising from model incompleteness. For example, referring back to Figure 4, suppose that the collisional excitation rate coefficient connecting levels 1 and 3 underestimated the actual value by a factor of two. Replacing the old rate coefficient in the 13-level model still neglects the 59% (formerly 67%) fraction of the influx from levels not in the model.

This problem can be addressed through hybridization of atomic models. A hybridization scheme might proceed along the following lines: construct a model that represents shells through, say, $n = 10$, where the atomic structure is broken out into detailed energy levels for the lowest few shells, then, moving to higher

shells, averaged down to something manageable, say jj-averaged or n-averaged (see Figure 6). Calculate all appropriate "level"-to-"level" radiative and collisional rates, using a fast distorted wave code for the latter. Some provision needs to be made for coupling to neighboring charge states, of course. With the addition of a superlevel, this constitutes a reasonably complete model (no more missing lines), with reasonably accurate rates. Now, work toward accuracy. As high-quality rates become available, substitute them into the working model, developing priorities based upon a reasonably complete treatment of the population kinetics.

As a final comment, I recommend that future assessments of atomic data quality invoke completeness as an essential criterion of merit.

Acknowledgements

I owe my appreciation to Tim Kallman and Manuel Bautista for their patience and cooperation. Kevin Fournier provided a number of useful comments on an early version of the text. This work was performed under the auspices of the U.S. Department of Energy by the University of California, Lawrence Livermore National Laboratory under Contract No. W-7405-Eng-48.

REFERENCES

1. Arnaud, M. & Raymond, J.C. 1992, ApJ, 398, 394.
2. Bar-Shalom, A., Klapisch, M., & Oreg, J. 1988, Phys. Rev. A, 38, 1773.
3. Beiersdorfer, P., et al. 1999, ApJ, 519, L185.
4. Brickhouse, N., Dupree, A., Edgar, R., Liedahl, D., Drake, S., White, N., & Singh, K. 2000, ApJ, 530, 387.
5. Brickhouse, N.S., Raymond, J.C., & Smith, B.W. 1995, ApJS, 97, 551.
6. Brinkman, A.C., et al. 2000, ApJ, 530, L111.
7. Canizares, C., et al. 2000, ApJ, submitted.
8. Dere, K.P., Mason, H.E., Widing, K.G., & Bhatia, A.K. 1979, ApJS, 40, 341.
9. Drake, J.J., Laming, J.M., & Widing, K.G. 1995, 443, 393.
10. Fawcett, B.C. & Mason, H.E. 1991, At. Data Nucl. Data Tables, 47, 17.
11. Feldman, U. 1992, ApJ, 385, 758.
12. Feldman, U., Doschek, G.A., & Widing, K.G. 1978, ApJ, 219, 304.
13. Haug, E. 1979, ApJ, 228, 903.
14. Klapisch, M., Schwab, J.L., Fraenkel, B.S., & Oreg, J. 1977, J. Opt. Soc. Am., 67, 148.
15. Liedahl, D.A., 1999, Phys. Scr., Vol. T83, 110.
16. McKenzie, D.L., Landecker, P.B., Broussard, R.M., Rugge, H.R., Young, R.M., & Doschek, G.A. 1980, ApJ, 241, 409.
17. Phillips, K.J.H., et al. 1982, ApJ, 256, 774.
18. Schmitt, J.H.M.M., Drake, J.J., & Stern, R.A. 1996, ApJ, 465, L51.